Supporting information

Understanding complex mechanisms of enzyme reactivity: the case of Limonene-1,2-epoxide hydrolases.

Silvia Rinaldi,[1] Marc W. Van der Kamp,[2,3] Kara E. Ranaghan,[2] Adrian J. Mulholland,[2*] Giorgio Colombo[1,4*]

[1] Istituto di Chimica del Riconoscimento Molecolare, C.N.R., Via Mario Bianco 9, 20131 Milano, Italy

[2] Centre for Computational Chemistry, School of Chemistry, University of Bristol, Cantock's Close, Bristol, BS8 1TS United Kingdom

[3] School of Biochemistry, University of Bristol, University Walk, Bristol, BS8 1TD United Kingdom

[4] Dipartimento di Chimica, Università degli Studi di Pavia, Via Taramelli 12, 27100 Pavia, Italy

Authors to whom correspondence should be addressed:

*Giorgio Colombo: g.colombo@unipv.it

*Adrian J. Mulholland: Adrian.Mulholland@bristol.ac.uk

Contents

Substrate Docking

The receptor and the ligands were first refined using the Schrodinger Maestro suite (Release 2013-1-9.4, Schrödinger, LLC, New York, NY, 2013) and then the catalytic site was mapped onto a grid with default parameters centered on the co-crystallized natural valpromide inhibitor, assuming that valpromide binds in a position similar to that of the LEH substrates (Figure S1).[1] As the valpromide carbonyl is found in hydrogen-bonding distance to Asp101 in the crystal structure, we defined the H-bond distance between the epoxide oxygen and the carboxylic acid as a positional constraint during the docking run. Docking calculations were performed using Glide,[2] keeping the receptor rigid and allowing flexibility for the ligands. Docking calculations were performed in Standard Precision mode (SP) with the OPLS-AA (2001) force field[3] using default settings. The best poses of the docking runs were selected using the Emodel empirical scoring function implemented in Maestro.

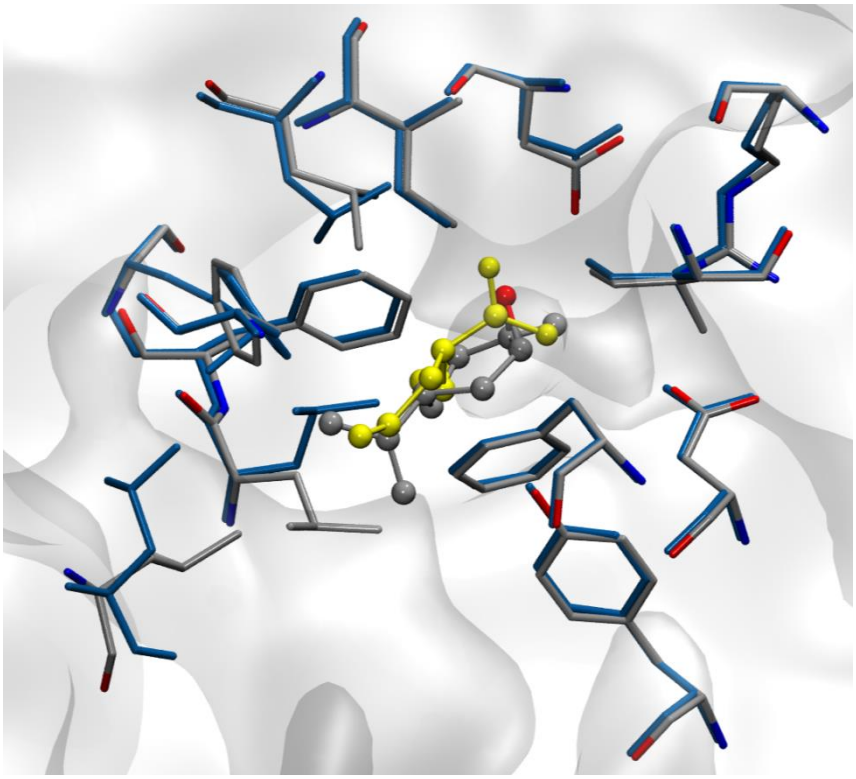

Figure S1. Comparison of the ligand cavity conformations in the presence (PDB code: 1nu3, VMD licorice representation) and in the absence (PDB code: 1nww, VMD blue licorice representation) of the inhibitor valpromide (yellow CPK VMD representation). The starting docking pose for limonene-1,2-epoxide is also shown (CPK VMD representation).

MD simulations

For all the simulations AMBER 12.0 package[4] was used with the AMBER ff99SB and with GAFF[5] for the ligands. Ligand parameters and AM1BCC partial charges were generated using Antechamber.[6] All the structures were solvated in a cuboid TIP3P water box[7] of dimensions of 77.4 Å X 67.5 Å X 65.7 Å . Counterions were added to ensure overall charge neutrality (15 Na^+ atoms) using the LeaP module of AMBER. The system was first minimized using the steepest descents algorithm. Secondly, a 0.4 ns simulation was run in the NVT ensemble in which the positions of α-carbons were weakly restrained (force constant, k = 10 kcal mol^{-1} $Å^{-2}$) and slowly increasing the temperature up to 300 K. Subsequently, a 0.2 ns simulation in the NPT ensemble was performed maintaining the same restraints. Finally, the whole system was simulated under NPT conditions for 100 ns (300 K, 1 atm) with a 1 fs time-step. All the simulations were performed applying periodic boundary conditions (PBC). Short-range electrostatic and van der Waals interactions were calculated within a 10 Å cutoff, whereas long-range electrostatic interactions were assessed using the particle Ewald method.[8] The Shake algorithm was used to treat all bonds involving hydrogen atoms.[9] PEO ligand shows a high mobility within itsbinding pocket, making the correct evaluation of the effects of PEO on LEH structures difficult. Thus, in order to correctly evaluate the effect of the PEO ligand on the enzyme dynamics and obtain an equilibrated starting structure for free energy calculations, we restrained PEO - Ash101 and the catalytic water - Asp132 to be within a hydrogen-bond distance in each case (a1 and a2 distance in figure S2, force constant, k =100 kcal mol^{-1} $Å^{-2}$) in monomer B (PEO-B). No restraints were placed on PEO in monomer A (PEO-A). The results of analysis by ProPKA[10] on the LEH crystal structure, assessed by visual inspection, were used to assign the protonation states of titratable residues. The catalytic Asp101 was predicted to be protonated in agreement with both experimental and computational investigations[1,11] and protonated Asp135 was predicted and used in LEH monomer B. The unique solvent exposed histidine (per monomer) was modeled as a positively charged residue (Hip85).

QM/MM simulations

QM/MM MD simulations (AM1/ff99SB) were run using the Sander code available in AMBER12 package.[4] In all cases, a neutral total charge is used for the QM region and 5 link atoms (LAs)[12,13] were used to saturate the QM atoms. The entire system was simulated in the NVT ensemble with a Langevin thermostat (300K).[14] The nonbonded interactions were computed using a cutoff of 10 Å. The system was simulated for 30 ps with a time step of 1 fs. QM/MM MD simulations were performed to

generate suitable structures for the free energy calculations. In order to sample the conformational ensemble around the catalytically active state, we used restraints to maintain the geometrical parameters that are reported to be fundamental for the enzyme catalysis.[11] One representative conformation per system was selected from the snapshots that fulfilled the following criteria: Hwat-OAsp132 (a1) < 2.0 Å, HAsh101-Oepoxide (a2) < 2.0 Å, Owat-Cepoxide (a3) < 3.5 Å, Hwat-OAsn55 (a4) < 2.0 Å (see Figure S2). An accurate estimation of the free energy profile would require the computation of multiple PMFs from different starting conformations. However, the cost of calculating multiple pathways is prohibitive due to the concerted nature of the reaction, requiring multidimensional sampling of reaction coordinates. PMFs (C1-LEO, C2-LEO and PEO) were obtained by performing 20 ps of biased QM/MM MD runs for each of the 266 windows of the Umbrella sampling space. Therefore, our assumption is that the starting, transition-state like conformations (obtained using the same geometrical criteria on each system), can provide the most reliable starting point for the estimation of the free energy barrier. 2D umbrella sampling QM/MM simulations (SCC-DFTB/ff99SB)[15] were performed along the two reaction coordinates (see Methods). The first reaction coordinate described the proton abstraction from the water molecule and the nucleophilic attack, defined as RC1= d1(Owat-Hwat)-d2(Owat-Clim), ranging from -2.2 to 0.4 Å by steps of 0.2 Å (see Figure S3). The second reaction coordinate accounted for the activation of the epoxide by proton transfer and the ring opening: RC2 = d3(Olim-Clim)-d4(Hash-Olim), ranging from -0.4 to 1.4 Å by steps of 0.1 Å (Figure S3). Umbrella sampling runs were performed sampling 20 ps at each window with a force constant of 200 kcal mol^{-1} $Å^{-2}$. Snapshots were taken after 10 ps of simulation as the starting point for the subsequent window. In order to reduce the computational time, the QM selection was limited to the side-chains of the catalytic triad (namely, Asp132, Ash101, and Arg99), the nucleophilic water molecule and the ligand. The SCC-DFTB method is known to favor proton transfer processes,[14] thus it was necessary to use mild restraints to avoid the deprotonation of Arg99. Without restraints we observed the deprotonation of Arg99 and a consequent conformational rearrangement which prevented the catalytic arginine bridging between the two aspartates. This would result in an inactive enzyme as demonstrated by experimental point mutations on Arg99.[1] Hence, when the distance between the arginine side-chain nitrogens and the respective hydrogen exceeded 1.2 Å a restraint (force constant k = 100 kcal mol^{-1} $Å^{-2}$) was applied. Using the transition state-like conformations located on the resulting 3D PMF surface as starting points, potential energy surfaces (PES) were obtained by adiabatic mapping along the reaction coordinates at the same level of theory (SCC-DFTB/ff99SB). Initially, each starting transition state structure was re-optimized with the reaction coordinates restrained by a harmonic potential (force constant, k = 1000 kcal mol^{-1} $Å^{-2}$) by 200 steps of steepest descents followed by conjugate gradient minimization. Subsequently, 10000 steps of LBFGS minimization[14] were performed with the reaction coordinates restrained by a harmonic potential (force

constant, k = 1000 kcal mol^{-1} Å^{-2}) until a gradient of 0.002 kcal mol^{-1} was reached. Using the resulting conformation, the same protocol was then used to map the potential energy surface, with the difference that mild restraints (force constant of 50 kcal mol^{-1} Å^{-2}) were applied to residues further than 8 Å from the QM region. The series of minimizations were run in both directions along the reaction coordinates by steps of 0.1 Å for both the RCs, using the minimized structure of the preceding step as the starting point. DFT QM/MM (B3LYP/6-31G*/ff99SB//SCC-DFTB/ff99SB) single point energy calculations (with electrostatic embedding) were finally performed on the geometries optimized at the lower QM/MM level, using the Orca package[14] implemented in Amber. The resulting 513 (27x19) point 3D PESs were ultimately used to give corrections along the reaction paths calculated at semi-empirical levels, as reported in ref[16]. Briefly, the difference between the activation energy calculated at SCC-DFTB/ff99SB and B3LYP/6-31G*/ff99SB level was divided by the number of points on the free energy profile between the reactant and the transition state, then the result was incrementally added to each point of the SCC-DFTB/ff99SB free energy profile.

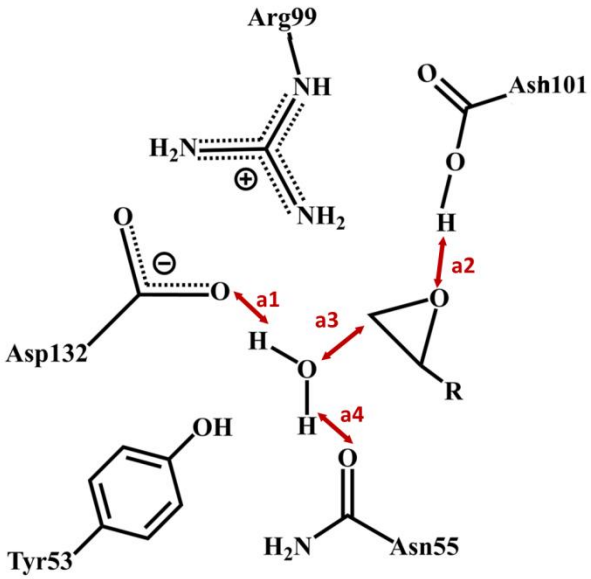

Figure S2. LEH Catalytic site and catalytically fundamental geometrical distances

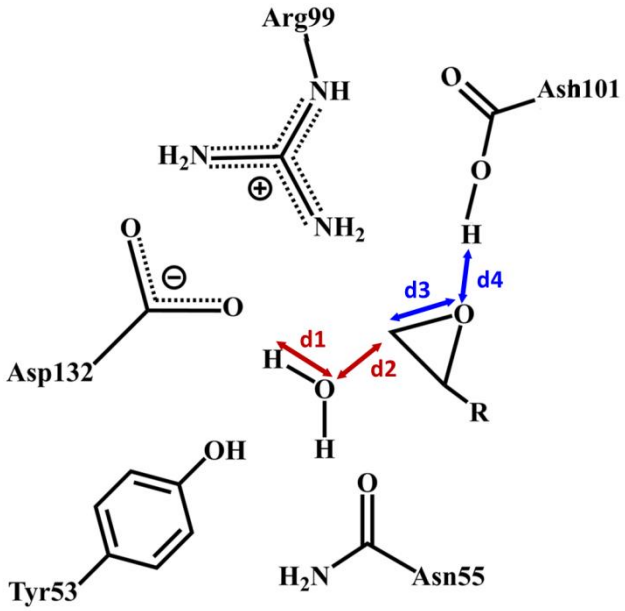

Figure S3. Representation of the distances used to define the RC1 (red arrows) and RC2 (blue arrows) reaction coordinates

WaterSwap calculations of substrate binding affinities

WaterSwap calculations[17] were performed in order to calculate the absolute protein-ligand binding free energies for the PEO and LEO systems. The calculations were run on structures resulting from cluster analysis of the MD trajectories. The cluster analysis was performed after alignment of the heavy atoms of the binding site (a 4 Å cavity around the QM atoms). Clustering based on the RMSD of the ligand was then carried out using the *ptraj* module of AmberTools[17] to obtain 5 clusters for each system. The most representative structure from each cluster was then used for *WaterSwap* calculations. The binding free energy of each ligand resulted from the weighted average of the representative structures obtained for both the dimer cavities. The standard *WaterSwap* protocol was used:[17] $\Delta\lambda$= 0.001, 1000 steps of iterations, 50.000 Monte Carlo moves for each window with a temperature of 298.15 K and pressure of 1 atm, while ligand translation and rotation motions were prevented. Final energies were obtained using the *analyse_freenrg* analysis method (available in Sire, https://siremol.org/index.html), which returns the binding energies averaging over the last 60% of iterations across the lambda windows. The absolute binding affinities for each conformation resulting from the cluster analysis are reported in Table S1.

Table S1. *WaterSwap* binding free energies computed on the most representative structures of LEO and PEO binding pockets with their relative weights on the conformational ensemble. The table reports also whether the conformation accounts for a reactive conformation or not. A reactive conformation is described as a state where: 1) at least one nucleophilic water molecule is within 4 Å of both one of the oxirane carbon atoms and an aspartate oxygen; 2) the protonated aspartic acid is within an H-bond distance from the oxirane oxygen.

	Coverage	Conformation	Binding Energy	Error
	%		kcal mol^{-1}	
PEO.A1	50.6	Reactive	-11.7	0.3
PEO.A2	40.1	Non-reactive	-11.0	0.3
PEO.A3	9.2	Non-reactive	-14.7	0.2
PEO.B1	88.2	Reactive	-11.8	0.4
PEO.B2	4.6	Non-reactive	-16.1	0.2
PEO.B3	4.4	Non-reactive	-12.2	0.2
LEO.A1	99.6	Reactive	-21.1	0.4
LEO.B1	99.3	Reactive	-24.5	0.1

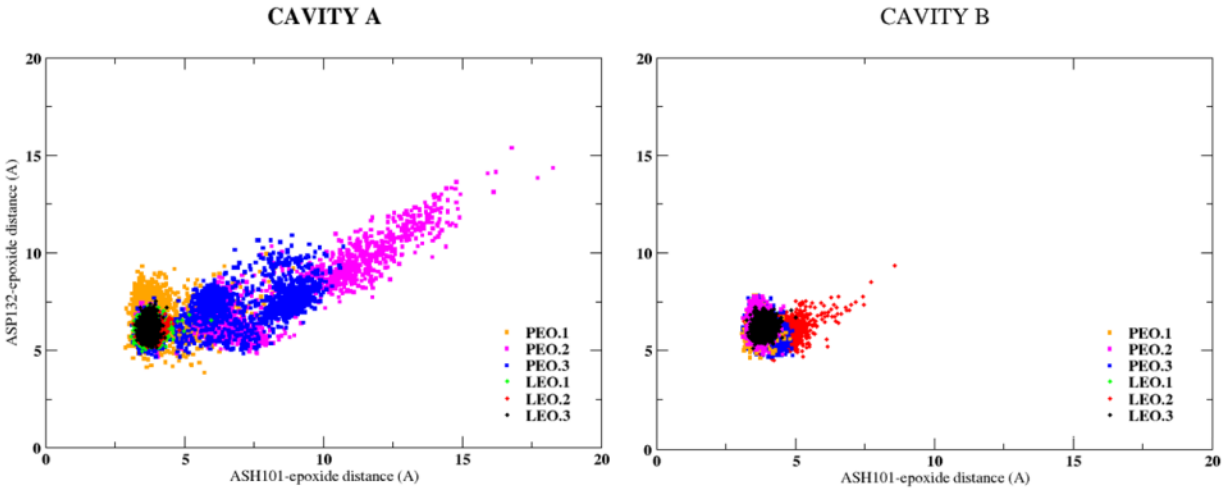

Figure S4. Evolution of ligand binding poses along 2 representative coordinates: the distance between Ash101-Cγ and epoxide-O and between Asp132-Cγ and epoxide-O for cavity A (PEO without restraints) and cavity B (PEO with restraints).

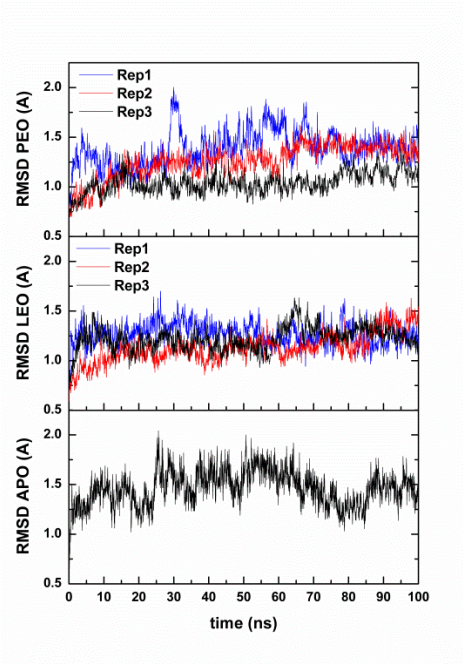

Figure S5. Time evolution of the RMSD (Å) of backbone atoms (N- and C-tails excluded) of all the replicate simulations of PEO, LEO and APO systems

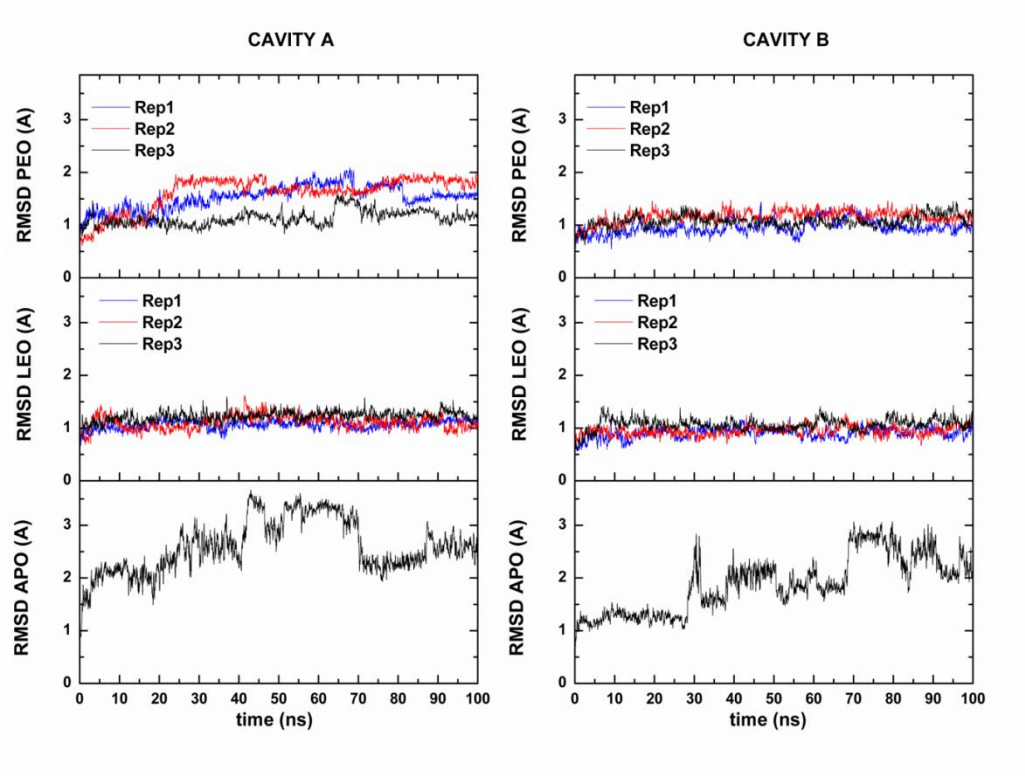

Figure S6. RMSD evolution (Å) of the heavy atoms of residues in the active site (defined as the residues that have at least one heavy atom within 4 Å of LEO in the X-ray structure) in monomer A (left) and B (right).

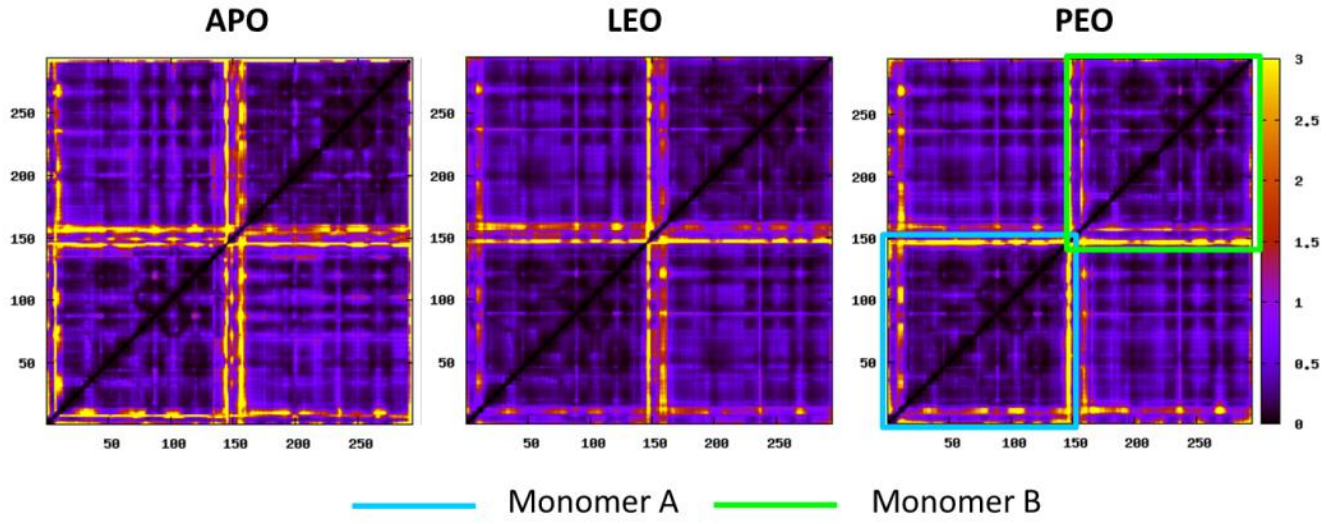

Figure S7. Long-range Communication Networks: Distance Fluctuation (Å^2) matrices (averaged on last 50 ns to 100 ns for all the replica simulations of each system). The long-range communication network is reported as a function of the distance fluctuations between residue pairs: any two residues are defined to be quasi-rigidly coordinated if their distance fluctuation is low (dark regions) or non-coordinated (flexible regions) if their distance fluctuation is high (yellow spots).

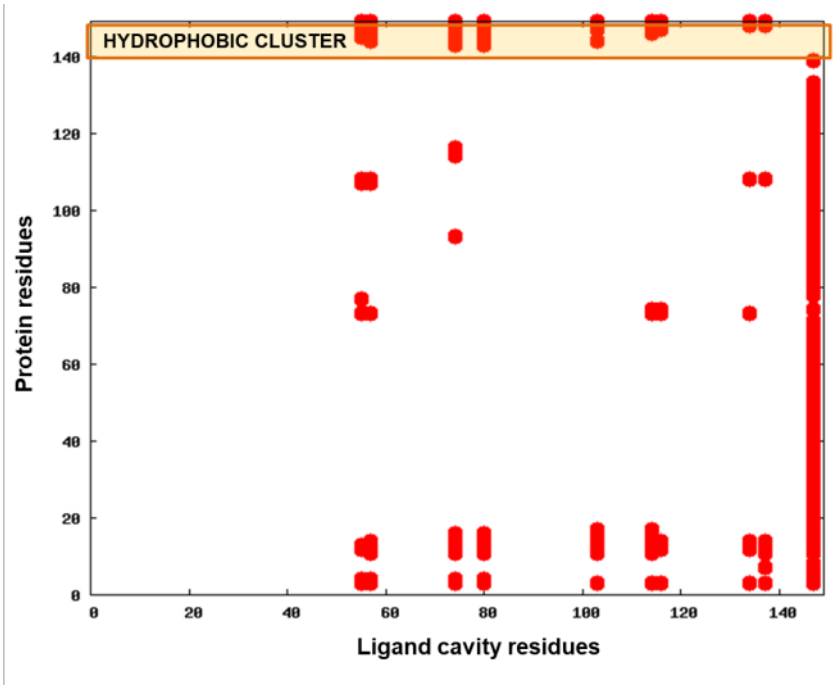

Figure S8. Residues of the ligand cavity whose dynamic coordination with the protein residues (identified by the red spots) is increased in the presence of LEO with respect of PEO.

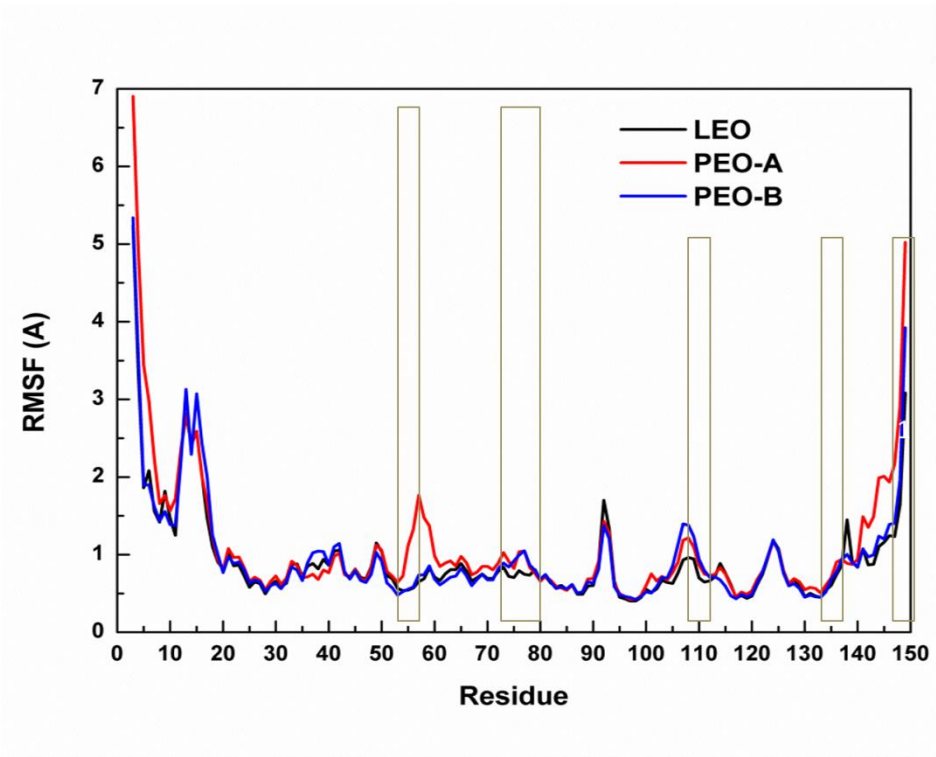

Figure S9. RMSF profiles for the LEO, PEO-A and PEO-B systems. Regions belonging to the ligand cavity are highlighted with the grey boxes.

MD simulations of models with ligands occupying a single monomer

As the enzyme may function with only one of the monomers occupied by a ligand, we built LEH models where the ligand was only bound to monomer A. Two independent 100ns MD simulations were performed on these models. For the PEO model, one of the simulations is performed restraining the ligand position to the active site, while the other simulation is unbiased (as in the PEO-A case). The resulting distance fluctuation matrices (Figure S10) show that the dynamics of monomer A (ligand bound monomer) in each case is similar to their double-occupancy counterpart. Monomer B profiles (where no ligand is bound) show larger mobility, in particular at the N- and C-tails. This reverberates on the Therefore, the monomer-monomer interaction patterns (out of diagonal regions) show intermediate properties between the apo and the doubly-occupied forms. However, the general internal dynamics behavior is not significantly affected by the presence of only one ligand. In particular, the monomer with a ligand bound shows internal dynamics properties consistent with those observed for the monomers in doubly occupied states. As the LEH crystal structure contained inhibitors in both monomers and there is little difference in the dynamics when only one monomer is

liganded, we have used the doubly-occupied models as our reference models described in the main text.

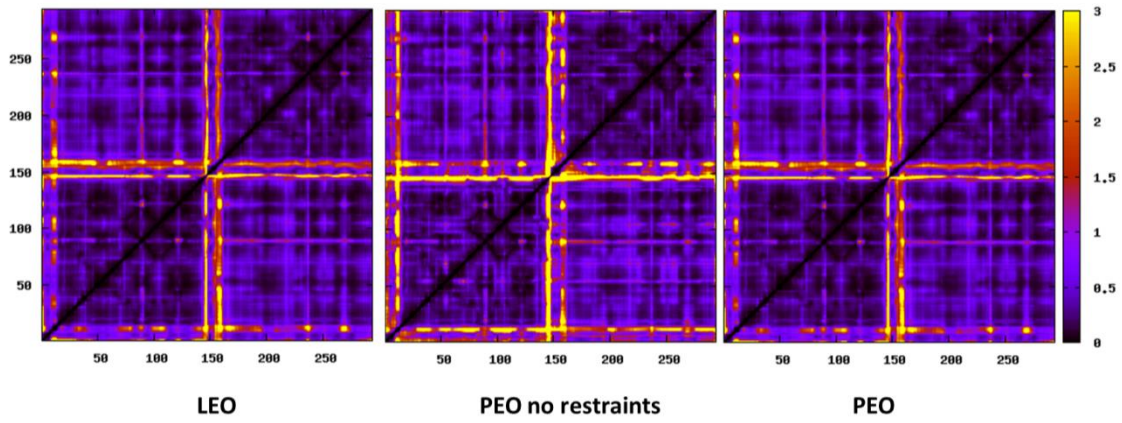

Figure S10. Long-range Communication Networks: Distance Fluctuation ($Å^2$) matrices for models where only monomer A is occupied by a ligand. The long-range communication network is reported as function of the distance fluctuations between residue pairs: any two residues are defined to be quasi-rigidly coordinated if their distance fluctuation is low (dark regions) or non-coordinated (flexible regions) if their distance fluctuation is high (yellow spots).

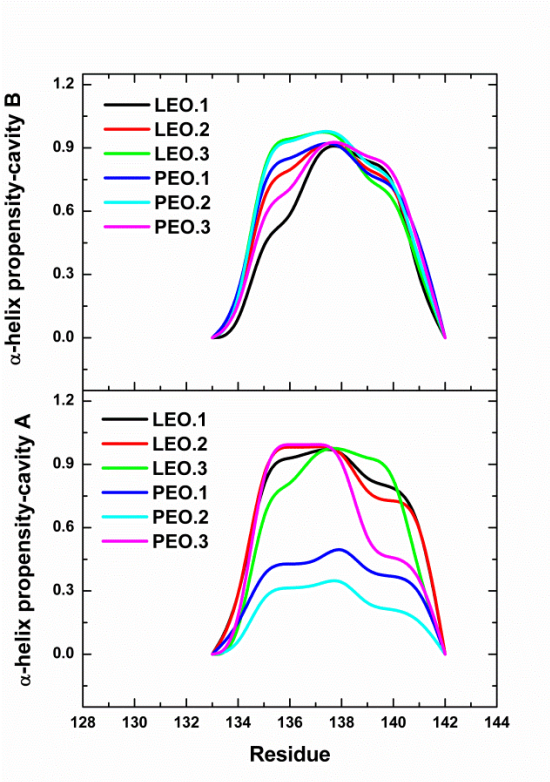

Figure S11. α-helix propensity of the C-terminal helix in the PEO and LEO systems (reported for all the 3 replicas)

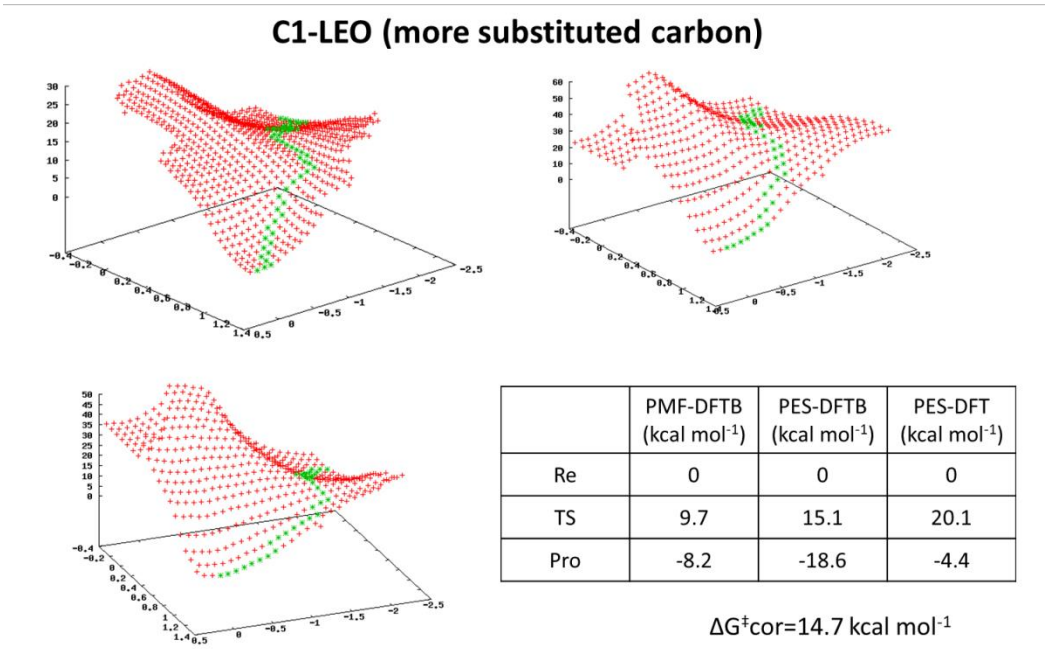

	PMF-DFTB (kcal mol^{-1})	PES-DFTB (kcal mol^{-1})	PES-DFT (kcal mol^{-1})
Re	0	0	0
TS	9.7	15.1	20.1
Pro	-8.2	-18.6	-4.4

$\Delta G^{\ddagger}$cor=14.7 kcal mol^{-1}

Figure S12. SCC-DFTB/ff99SB PMF (top left), SCC-DFTB/ff99SB PES (top right) and B3LYP/6-31G*/ff99SB//SCC-DFTB/ff99SB PES (bottom left) for C1-LEO system. Green points report the corresponding Minimum Energy Path (MEP). Bottom right. Energy values obtained from the MEPs. The value of the corrected free energy barrier (B3LYP/6-31G*/ff99SB//SCC-DFTB/ff99SB) is reported ($\Delta G^{\ddagger}_{cor}$).

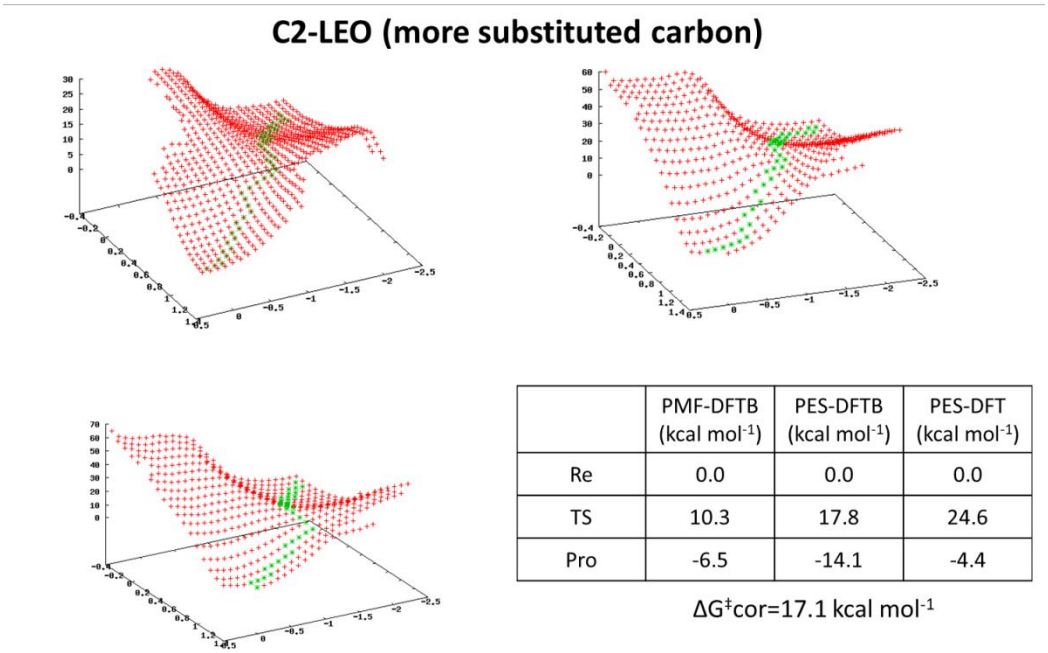

	PMF-DFTB (kcal mol^{-1})	PES-DFTB (kcal mol^{-1})	PES-DFT (kcal mol^{-1})
Re	0.0	0.0	0.0
TS	10.3	17.8	24.6
Pro	-6.5	-14.1	-4.4

$\Delta G^{\ddagger}$cor=17.1 kcal mol^{-1}

Figure S13. SCC-DFTB/ff99SB PMF (top left), SCC-DFTB/ff99SB PES (top right) and B3LYP/6-31G*/ff99SB//SCC-DFTB/ff99SB PES (bottom left) for C2-LEO system. Green points report the corresponding Minimum Energy Path (MEP).

Bottom right. Energy values obtained from the MEPs. The value of the corrected free energy barrier (B3LYP/6-31G*/ff99SB//SCC-DFTB/ff99SB) is reported ($\Delta G^{\ddagger}_{cor}$).

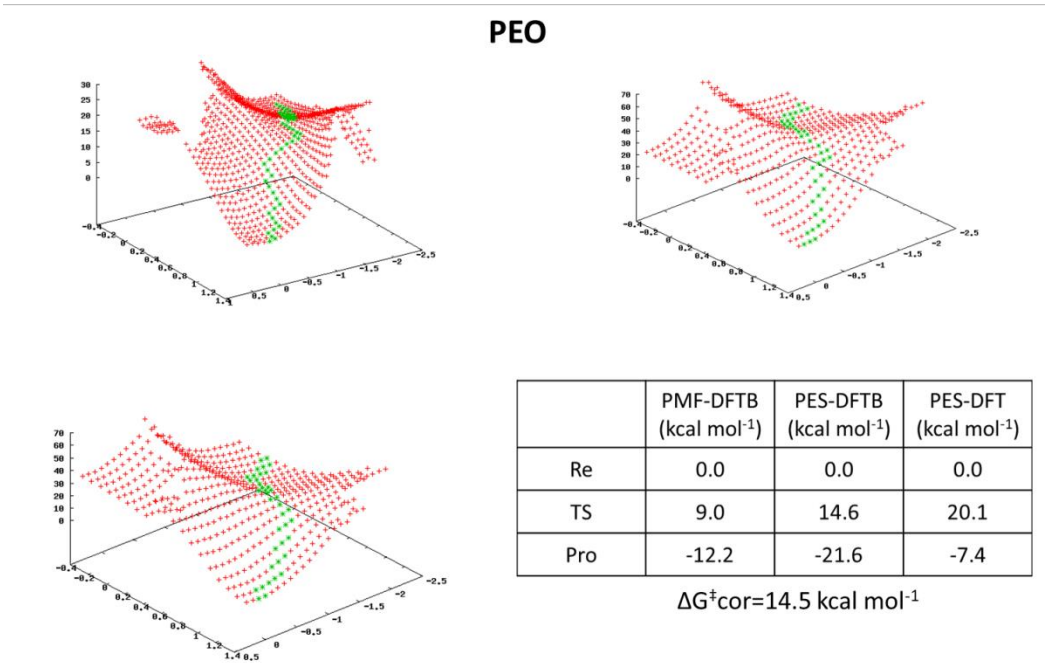

Figure S14. SCC-DFTB/ff99SB PMF (top left), SCC-DFTB/ff99SB PES (top right) and B3LYP/6-31G*/ff99SB//SCC-DFTB/ff99SB PES (bottom left) for PEO system. Green points report the corresponding Minimum Energy Path (MEP). Bottom right. Energy values obtained from the MEPs. The value of the corrected free energy barrier (B3LYP/6-31G*/ff99SB//SCC-DFTB/ff99SB) is reported ($\Delta G^{\ddagger}_{cor}$).

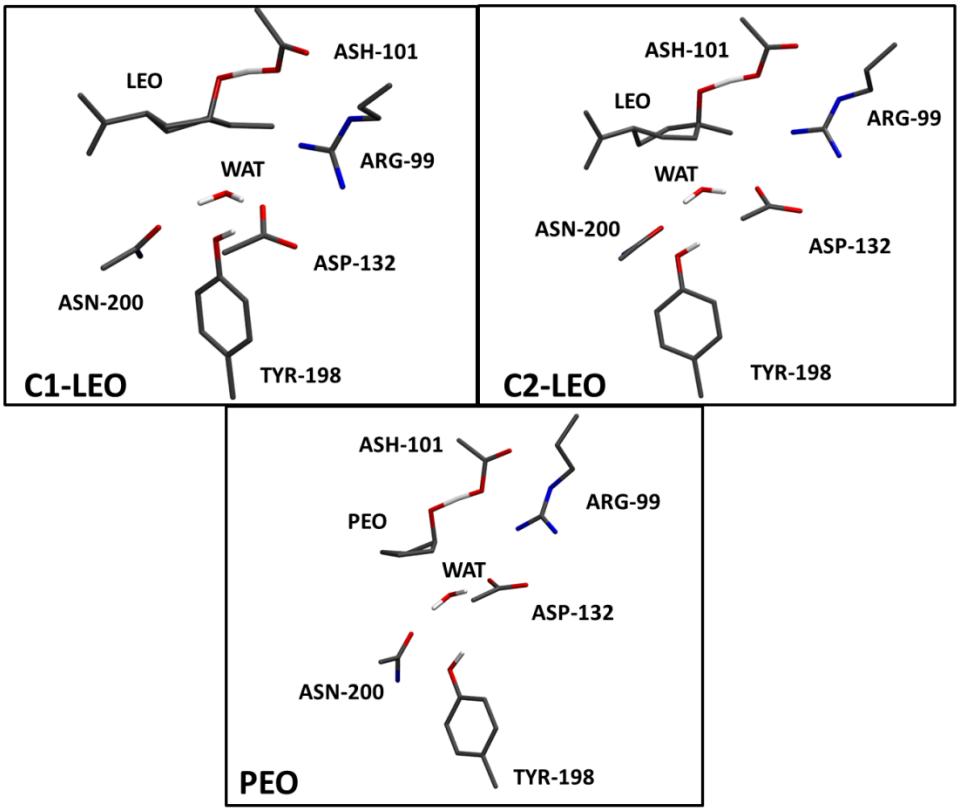

Figure S15. Conformations of the TSs catalytic pockets in C1-LEO, C2-LEO and PEO.

Table S2. Structural parameters of the reactant, transition state and product in C1-LEO, C2-LEO and PEO.

		C6-C5 (Å)	C4-C5 (Å)	C3-C4 (Å)	C1-C6 (Å)	C1-C2 (Å)	C2-C3 (Å)	C1-C7 (Å)	C1-O (Å)	C2-O (Å)	C4-C8 (Å)
LEO-C1	Re	1.52	1.52	1.53	1.51	1.48	1.50	1.50	1.51	1.49	1.51
	TS	1.52	1.52	1.53	1.49	1.48	1.52	1.48	2.06	1.47	1.51
	Pro	1.51	1.52	1.53	1.53	1.52	1.52	1.52	2.35	1.43	1.51
LEO-C2	Re	1.52	1.52	1.53	1.52	1.48	1.50	1.50	1.50	1.49	1.51
	TS	1.52	1.52	1.53	1.53	1.48	1.49	1.51	1.48	2.02	1.51
	Pro	1.52	1.52	1.53	1.54	1.54	1.52	1.52	1.45	2.41	1.51

		C4-C5 (Å)	C3-C4 (Å)	C1-C5 (Å)	C1-C2 (Å)	C2-C3 (Å)	C1-O (Å)	C2-O (Å)
PEO	Re	1.53	1.53	1.50	1.47	1.51	1.49	1.49
	TS	1.53	1.52	1.49	1.48	1.52	2.03	1.46
	Pro	1.53	1.52	1.52	1.53	1.52	2.42	1.43

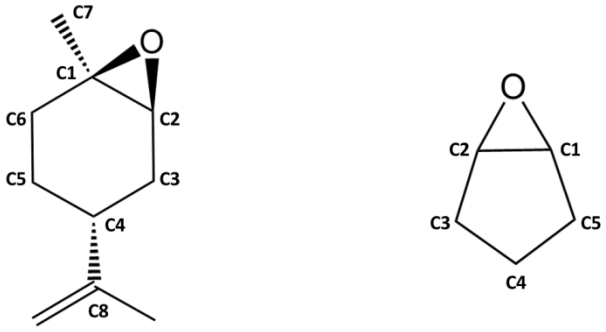

Table S3. Evolution of structural parameters associated to the catalytic mechanism along the MEPs.

		Owat-Cepo (Å)	Cepo-Oepo (Å)	Oepo-Hash (Å)	Hash-Oash (Å)	Owat-Hwat (Å)	Hwat-Oasp (Å)	Owat-Htyr (Å)	Hwat-Oasn (Å)	Cash-Carg (Å)	Casp-Carg (Å)	Owat-Cepo-Cepo (°)	Owat-Cepo-Oepo (°)
LEO-C1	Re	3.19	1.51	1.71	1.01	0.99	1.79	1.95	1.76	4.18	3.87	77.9	136.4
	TS	2.38	2.06	1.26	1.18	0.99	1.72	2.22	1.74	4.09	3.89	98.4	143.2
	Pro	1.50	2.35	1.04	1.73	1.61	1.03	2.61	1.82	3.91	4.05	109.0	144.5
LEO-C2	Re	3.29	1.49	1.79	1.01	0.99	1.80	1.94	1.73	4.18	3.90	82.1	140.1
	TS	2.11	2.02	1.32	1.15	1.01	1.66	2.69	1.68	4.08	3.93	102.7	148.0
	Pro	1.49	2.41	1.01	1.76	1.49	1.05	3.18	1.70	3.91	4.08	108.7	143.4
PEO	Re	3.19	1.50	1.69	1.01	0.99	1.81	1.99	1.74	4.22	3.91	95.9	148.7
	TS	2.10	2.00	1.33	1.13	1.00	1.68	2.72	1.73	4.12	3.95	109.2	150.9
	Pro	1.49	2.40	1.01	1.75	1.59	1.03	3.24	1.73	3.95	4.11	109.9	140.7

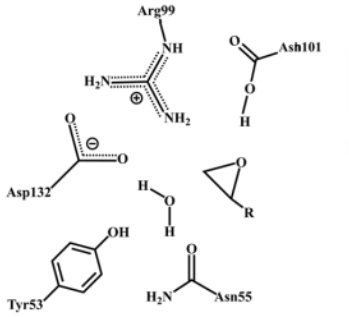

Table S4. Partial atomic charges from Mulliken population analysis (with charges summed on heavy atoms) of the QM atoms along the MEPs from B3LYP/6-31G*/ff99SB//SCC-DFTB/ff99SB) single point energy calculations. Different residues are reported according to different color codes.

		C1-LEO			C2-LEO					PEO			
		Re	TS	Pro	Re	TS	Pro			Re	TS	Pro	
C	1	0.20	0.19	0.18	0.20	0.19	0.18	C	1	0.20	0.19	0.18	
N	4	-0.21	-0.20	-0.17	-0.21	-0.20	-0.17	N	4	-0.22	-0.21	-0.18	
C	6	0.75	0.74	0.74	0.74	0.74	0.74	C	6	0.75	0.74	0.74	ARG99
N	7	-0.05	-0.05	-0.07	-0.05	-0.05	-0.07	N	7	-0.04	-0.05	-0.07	
N	10	-0.04	-0.05	-0.05	-0.04	-0.05	-0.05	N	10	-0.05	-0.05	-0.06	
C	13	0.05	0.01	-0.02	0.03	0.00	-0.04	C	13	0.02	0.00	-0.05	
C	16	0.59	0.59	0.58	0.59	0.59	0.58	C	16	0.59	0.59	0.58	ASH101
O	17	-0.44	-0.48	-0.56	-0.43	-0.48	-0.57	O	17	-0.43	-0.48	-0.56	
O	18	-0.64	-0.66	-0.59	-0.63	-0.65	-0.59	O	18	-0.63	-0.65	-0.59	
H	19	0.47	0.49	0.45	0.46	0.48	0.44	H	19	0.47	0.49	0.44	
C	20	-0.06	-0.06	0.01	-0.06	-0.06	0.00	C	20	-0.06	-0.06	0.01	
C	23	0.56	0.56	0.59	0.56	0.57	0.59	C	23	0.56	0.56	0.59	ASP132
O	24	-0.59	-0.58	-0.47	-0.60	-0.58	-0.48	O	24	-0.59	-0.58	-0.46	
O	25	-0.59	-0.60	-0.14	-0.59	-0.60	-0.13	O	25	-0.59	-0.60	-0.14	
C	6	0.00	0.06	0.03	0.00	0.01	0.01	C	3	0.05	0.04	0.01	
C	5	0.02	0.01	-0.04	0.01	-0.01	-0.03						
C	4	-0.02	0.00	0.02	0.00	0.03	0.03	C	4	0.00	0.02	0.01	
C	3	0.03	0.02	-0.02	0.03	0.04	-0.02	C	5	0.05	0.05	-0.02	
C	1	0.34	0.38	0.32	0.34	0.35	0.32	C	2	0.25	0.26	0.26	EPO
O	32	-0.57	-0.67	-0.25	-0.57	-0.69	-0.29	O	28	-0.55	-0.66	-0.27	
C	8	0.02	0.02	0.01	0.02	0.02	0.01						
C	2	0.22	0.24	0.22	0.23	0.25	0.24	C	1	0.26	0.28	0.26	
O	53	-0.93	-0.88	-0.75	-0.93	-0.83	-0.73	O	40	-0.93	-0.82	-0.74	
H	54	0.45	0.47	0.48	0.45	0.48	0.49	H	41	0.44	0.46	0.48	WAT
H	55	0.45	0.46	0.47	0.45	0.46	0.49	H	42	0.45	0.48	0.49	

Cartesian Coordinates of Reactant, Transition State and Product structures from the B3LYP/6-31G*/ff99SB//SCC-DFTB/ff99SB PES.

C1-LEO Re

C	39.013093	15.558988	23.530540
H	39.562673	14.656412	23.218301
H	38.877331	15.502775	24.617960
N	37.753171	15.584924	22.835537
H	37.832808	15.582371	21.789271
C	36.582193	16.039749	23.345902
N	36.398790	16.302880	24.651498
H	37.172802	16.226069	25.319069
H	35.475949	16.736715	24.963067
N	35.554322	16.167794	22.495946
H	35.714899	15.999290	21.489263
H	34.603356	16.535172	22.844433
C	37.510909	16.401541	17.777440
H	37.306651	17.473966	17.656734
H	36.751941	15.864816	17.196058
C	37.366827	16.042402	19.236089
O	38.234795	16.133716	20.089131
O	36.123245	15.603613	19.636487
H	35.351439	15.821443	19.014938
C	32.642059	19.289653	24.281273
H	31.607302	19.162231	23.942646
H	33.156521	19.870734	23.500846
C	33.361681	17.936680	24.349237

O	34.085521	17.602975	25.349594
O	33.246858	17.201252	23.294317
C	31.373833	15.347662	18.551667
C	30.437434	16.535200	18.449231
C	31.196399	17.769141	17.981551
C	32.178590	18.211984	19.067411
C	33.027732	14.595960	20.346240
C	32.598521	15.663341	19.383701
O	33.747519	16.270048	18.607621
C	30.289480	18.918733	17.603496
C	30.839088	19.864019	16.585991
C	29.067712	19.095249	18.126357
H	30.840708	14.492823	19.006912

C1-LEO TS

C	39.004305	15.556544	23.491386
H	39.553729	14.655673	23.173401
H	38.863323	15.490099	24.578517
N	37.750537	15.595894	22.787100
H	37.838702	15.625582	21.730873
C	36.588870	16.070858	23.289625
N	36.390315	16.304161	24.601206
H	37.151622	16.188124	25.277028
H	35.472088	16.730500	24.918685
N	35.581076	16.256064	22.424379
H	35.751753	16.097956	21.405377
H	34.641290	16.596332	22.778857

C	37.413800	16.422268	17.786760
H	37.213717	17.493178	17.648894
H	36.667047	15.883086	17.191822
C	37.224269	16.077675	19.253527
O	38.133341	16.121021	20.092516
O	35.978090	15.741404	19.651525
H	35.020218	16.080438	19.046856
C	32.642965	19.274830	24.272599
H	31.609950	19.170687	23.920957
H	33.180662	19.842088	23.497922
C	33.331405	17.903987	24.361660
O	34.062921	17.583162	25.355814
O	33.183894	17.138311	23.328269
C	31.237193	15.445168	18.973358
C	30.371447	16.642436	18.633495
C	31.207902	17.776577	18.057880
C	32.247775	18.236749	19.082396
C	33.060867	14.719377	20.588665
C	32.398080	15.803503	19.829401
O	33.904788	16.444627	18.575018
C	30.363002	18.949127	17.607658
C	30.979767	19.830655	16.572371
C	29.131954	19.199010	18.077297
H	30.638975	14.661325	19.475683

C1-LEO Pro

C	39.050939	15.551086	23.367781
H	39.609156	14.672008	23.007543
H	38.891278	15.414088	24.447990

N	37.819109	15.640723	22.631762
H	37.947046	15.791568	21.527741
C	36.659810	16.060271	23.147495
N	36.460896	16.233917	24.482826
H	37.239039	16.145958	25.142523
H	35.570431	16.635003	24.825373
N	35.642111	16.273399	22.294195
H	35.798843	16.080688	21.244925
H	34.714590	16.528929	22.660476
C	37.488959	16.428584	17.806781
H	37.293188	17.498685	17.654476
H	36.734198	15.885681	17.224494
C	37.286420	16.110889	19.288514
O	38.240961	16.236368	20.124588
O	36.087322	15.783700	19.661821
H	34.564340	16.210715	18.972142
C	32.615337	19.179409	24.275361
H	31.587889	19.056522	23.917247
H	33.173609	19.686779	23.475408
C	33.280959	17.841642	24.501711
O	34.067451	17.593430	25.415048
O	33.065302	16.871073	23.580096
C	30.917781	15.633712	19.400598
C	30.115860	16.805926	18.879766
C	31.012923	17.832283	18.202037
C	32.112278	18.293719	19.160735
C	32.827821	14.856584	20.808241
C	32.027321	16.064031	20.356347
O	33.604656	16.448037	18.662420
C	30.240286	19.017659	17.666352

C	30.927308	19.817263	16.608226
C	29.006049	19.350173	18.074864
H	30.248881	14.909464	19.903113

C2-LEO Re

C	38.334047	15.560224	23.661941
H	38.854145	14.642527	23.344479
H	38.202578	15.507186	24.749998
N	37.067744	15.619544	22.978346
H	37.126412	15.552511	21.934758
C	35.901613	16.084245	23.488497
N	35.737653	16.413574	24.782147
H	36.516052	16.353153	25.447024
H	34.810440	16.838993	25.085813
N	34.851533	16.155717	22.656470
H	34.995257	15.961878	21.652869
H	33.923075	16.598622	22.983124
C	36.774838	16.650507	17.963332
H	36.604492	17.736056	17.959272
H	36.001554	16.207321	17.326066
C	36.621597	16.134546	19.374897
O	37.501561	16.088624	20.217880
O	35.358873	15.721186	19.733353
H	34.622545	15.995004	19.103398
C	31.986393	19.442040	24.416900
H	30.966573	19.346109	24.027019

H	32.539215	20.063358	23.696146
C	32.688142	18.075281	24.435136
O	33.370466	17.672600	25.440542
O	32.603599	17.402387	23.336488
C	30.605147	15.669174	18.390568
C	29.712017	16.889915	18.286003
C	30.532032	18.139520	17.996903
C	31.411369	18.461448	19.206693
C	32.130358	14.742738	20.222284
C	31.782710	15.890009	19.317966
O	32.976049	16.536641	18.674437
C	29.682312	19.339103	17.639061
C	30.336749	20.369460	16.778188
C	28.420400	19.492687	18.066241
H	30.015748	14.809427	18.760409

C2-LEO TS

C	38.329443	15.552371	23.624121
H	38.849930	14.638294	23.296763
H	38.195088	15.485477	24.712066
N	37.068024	15.624098	22.934446
H	37.131757	15.594752	21.878491
C	35.907396	16.088737	23.443933
N	35.734074	16.388371	24.747455
H	36.509092	16.313636	25.414339
H	34.818035	16.815641	25.058657
N	34.866921	16.195482	22.602437

H	35.014135	16.021607	21.584259
H	33.946816	16.587227	22.947657
C	36.665024	16.653292	17.981602
H	36.491857	17.737456	17.963012
H	35.904773	16.204987	17.333817
C	36.477836	16.152383	19.402991
O	37.399271	16.088768	20.226230
O	35.233092	15.806277	19.785495
H	34.305329	16.105520	19.167470
C	31.996738	19.440268	24.436452
H	30.981705	19.359784	24.030503
H	32.575625	20.041656	23.719213
C	32.667755	18.058271	24.488118
O	33.376149	17.683221	25.475744
O	32.527046	17.335900	23.419700
C	30.775767	15.657449	18.448927
C	29.823335	16.831406	18.332831
C	30.597532	18.117715	18.088755
C	31.405445	18.463573	19.343433
C	32.302109	14.755289	20.236819
C	31.971905	15.945426	19.362114
O	33.152908	16.444188	18.621613
C	29.722015	19.288452	17.698010
C	30.359972	20.320531	16.826956
C	28.451898	19.415046	18.109808
H	30.223863	14.779426	18.834109

C2-LEO Pro

C	38.329443	15.552371	23.624121

H	38.849930	14.638294	23.296763
H	38.195088	15.485477	24.712066
N	37.068024	15.624098	22.934446
H	37.131757	15.594752	21.878491
C	35.907396	16.088737	23.443933
N	35.734074	16.388371	24.747455
H	36.509092	16.313636	25.414339
H	34.818035	16.815641	25.058657
N	34.866921	16.195482	22.602437
H	35.014135	16.021607	21.584259
H	33.946816	16.587227	22.947657
C	36.665024	16.653292	17.981602
H	36.491857	17.737456	17.963012
H	35.904773	16.204987	17.333817
C	36.477836	16.152383	19.402991
O	37.399271	16.088768	20.226230
O	35.233092	15.806277	19.785495
H	34.305329	16.105520	19.167470
C	31.996738	19.440268	24.436452
H	30.981705	19.359784	24.030503
H	32.575625	20.041656	23.719213
C	32.667755	18.058271	24.488118
O	33.376149	17.683221	25.475744
O	32.527046	17.335900	23.419700
C	30.775767	15.657449	18.448927
C	29.823335	16.831406	18.332831
C	30.597532	18.117715	18.088755
C	31.405445	18.463573	19.343433
C	32.302109	14.755289	20.236819
C	31.971905	15.945426	19.362114

O	33.152908	16.444188	18.621613
C	29.722015	19.288452	17.698010
C	30.359972	20.320531	16.826956
C	28.451898	19.415046	18.109808
H	30.223863	14.779426	18.834109

PEO Re

C	44.455251	20.592263	18.117760
H	44.665552	20.383568	17.057692
H	45.190639	21.330360	18.463738
N	44.559276	19.358925	18.854161
H	43.973356	18.575968	18.484584
C	45.051278	19.213043	20.108272
N	45.688144	20.191403	20.772630
H	45.846422	21.109607	20.344806
H	45.992062	20.011954	21.774880
N	44.926644	18.004620	20.681739
H	44.358837	17.285608	20.208498
H	45.197667	17.860087	21.716241
C	40.864095	15.829841	18.302314
H	40.232594	15.927894	19.194506
H	41.095066	14.763598	18.183249
C	42.159208	16.591605	18.499310
O	42.469470	17.631812	17.943019
O	43.050822	16.032404	19.377030
H	42.666403	15.272084	19.922856

C	45.041358	18.741114	25.357062
H	45.283615	17.820260	25.901089
H	43.948558	18.750343	25.230165
C	45.633210	18.701685	23.938672
O	46.257783	19.693222	23.432555
O	45.376245	17.620572	23.278179
C	43.051010	14.516261	22.427044
C	43.503727	13.378842	21.604889
O	42.326438	14.176448	21.167124
C	43.091714	12.094350	22.272780
C	42.338147	13.986239	23.640570
C	42.058928	12.520883	23.314981
H	44.367773	13.422826	20.916406
H	42.683504	11.355206	21.560151
H	42.096396	11.882590	24.215099
H	43.974652	11.630936	22.750341
H	41.043146	12.418003	22.893859
H	43.001882	14.079181	24.516022
H	41.413534	14.543396	23.867098

PEO TS

C	44.435862	20.564960	18.108273
H	44.643812	20.358429	17.047258
H	45.178503	21.296029	18.455526
N	44.524709	19.328066	18.839997
H	43.905713	18.554491	18.477185

C	45.016682	19.176778	20.088280
N	45.679068	20.144872	20.749310
H	45.849249	21.060474	20.320801
H	45.981711	19.965920	21.745412
N	44.869242	17.971999	20.667361
H	44.270637	17.260153	20.202669
H	45.162484	17.828209	21.675726
C	40.898286	15.818436	18.347546
H	40.260387	15.908416	19.235670
H	41.132470	14.753240	18.227418
C	42.196116	16.584595	18.563928
O	42.495566	17.622083	17.964779
O	43.053573	16.073704	19.466165
H	42.649559	15.224784	20.098825
C	45.028649	18.716847	25.363993
H	45.258009	17.802148	25.924072
H	43.937039	18.735635	25.228088
C	45.635596	18.652839	23.951789
O	46.243823	19.638923	23.432009
O	45.406630	17.547192	23.308106
C	43.322985	14.710894	22.616325
C	43.476169	13.693833	21.549843
O	42.280155	14.257632	20.932309
C	43.152456	12.359722	22.195526
C	42.409473	14.173068	23.661567
C	42.132946	12.719888	23.270196

H	44.373366	13.720451	20.882506
H	42.754597	11.629918	21.470764
H	42.186651	12.040980	24.140191
H	44.064235	11.922556	22.642333
H	41.112590	12.634668	22.859032

PEO Pro

C	44.367307	20.495211	17.996810
H	44.537172	20.288560	16.929424
H	45.140830	21.208338	18.317863
N	44.434909	19.256108	18.723361
H	43.727944	18.482444	18.397119
C	44.976902	19.096262	19.935422
N	45.717602	20.058534	20.546773
H	45.897417	20.957908	20.090664
H	46.064989	19.914955	21.508507
N	44.807445	17.907758	20.544326
H	44.112722	17.191677	20.135248
H	45.199553	17.761173	21.485636
C	40.918388	15.786420	18.388442
H	40.257217	15.840496	19.262461
H	41.166421	14.727126	18.240902
C	42.218997	16.561025	18.675517
O	42.521886	17.582782	17.983076
O	42.962932	16.128476	19.644781
H	43.139343	14.560801	20.402070

C	45.091709	18.767805	25.260644
H	45.293571	17.828589	25.788640
H	44.018068	18.776030	25.024331
C	45.841606	18.820544	23.948404
O	46.339074	19.823517	23.448370
O	45.908310	17.658930	23.245695
C	43.648122	14.910622	22.891856
C	44.128194	13.787472	21.976136
O	43.230412	13.664486	20.865248
C	44.017677	12.536816	22.838806
C	42.569662	14.282238	23.762963
C	42.788031	12.769585	23.707805
H	45.182115	13.965157	21.613904
H	43.931002	11.621078	22.231501
H	42.914442	12.340361	24.717823
H	44.920257	12.431355	23.468355
H	41.906158	12.275034	23.265424
H	42.626245	14.664076	24.793452
H	41.569721	14.547182	23.381726

References

(1) Arand, M.; Hallberg, B. M.; Zou, J.; Bergfors, T.; Oesch, F.; Werf, M. J. van der; Bont, J. A. M. de; Jones, T. A.; Mowbray, S. L. Structure of Rhodococcus Erythropolis Limonene-1,2-Epoxide Hydrolase Reveals a Novel Active Site. *EMBO J.* **2003**, *22*, 2583–2592.

(2) Friesner, R. A.; Banks, J. L.; Murphy, R. B.; Halgren, T. A.; Klicic, J. J.; Mainz, D. T.; Repasky, M. P.; Knoll, E. H.; Shelley, M.; Perry, J. K.; Shaw, D. E.; Francis, P.; Shenkin, P. S. Glide: A

New Approach for Rapid, Accurate Docking and Scoring. 1. Method and Assessment of Docking Accuracy. *J. Med. Chem.* **2004**, *47*, 1739–1749.

(3) Kaminski, G. A.; Friesner, R. A.; Tirado-Rives, J.; Jorgensen, W. L. Evaluation and Reparametrization of the OPLS-AA Force Field for Proteins via Comparison with Accurate Quantum Chemical Calculations on Peptides. *J. Phys. Chem. B* **2001**, *105*, 6474–6487.

(4) Pearlman, D. A.; Case, D. A.; Caldwell, J. W.; Ross, W. S.; Cheatham, T. E.; DeBolt, S.; Ferguson, D.; Seibel, G.; Kollman, P. AMBER, a Package of Computer Programs for Applying Molecular Mechanics, Normal Mode Analysis, Molecular Dynamics and Free Energy Calculations to Simulate the Structural and Energetic Properties of Molecules. *Comput. Phys. Commun.* **1995**, *91*, 1–41.

(5) Wang, J.; Wolf, R. M.; Caldwell, J. W.; Kollman, P. A.; Case, D. A. Development and Testing of a General Amber Force Field. *J. Comput. Chem.* **2004**, *25*, 1157–1174.

(6) Hornak, V.; Abel, R.; Okur, A.; Strockbine, B.; Roitberg, A.; Simmerling, C. Comparison of Multiple Amber Force Fields and Development of Improved Protein Backbone Parameters. *Proteins Struct. Funct. Bioinforma.* **2006**, *65*, 712–725.

(7) Jorgensen, W. L.; Chandrasekhar, J.; Madura, J. D.; Impey, R. W.; Klein, M. L. Comparison of Simple Potential Functions for Simulating Liquid Water. *J. Chem. Phys.* **1983**, *79*, 926.

(8) Darden, T.; York, D.; Pedersen, L. Particle Mesh Ewald: An N· log(N) Method for Ewald Sums in Large Systems. *J. Chem. Phys.* **1993**, *98*, 10089.

(9) Ryckaert, J.-P.; Ciccotti, G.; Berendsen, H. J. . Numerical Integration of the Cartesian Equations of Motion of a System with Constraints: Molecular Dynamics of N-Alkanes. *J. Comput. Phys.* **1977**, *23*, 327–341.

(10) Bas, D. C.; Rogers, D. M.; Jensen, J. H. Very Fast Prediction and Rationalization of pKa Values for Protein-Ligand Complexes. *Proteins* **2008**, *73*, 765–783.

(11) Hopmann, K. H.; Hallberg, B. M.; Himo, F. Catalytic Mechanism of Limonene Epoxide Hydrolase, a Theoretical Study. *J. Am. Chem. Soc.* **2005**, *127*, 14339–14347.

(12) Reuter, N.; Dejaegere, A.; Maigret, B.; Karplus, M. Frontier Bonds in QM/MM Methods: A Comparison of Different Approaches. *J. Phys. Chem. A* **2000**, *104*, 1720–1735.

(13) Field, M. J.; Bash, P. A.; Karplus, M. A Combined Quantum Mechanical and Molecular

Mechanical Potential for Molecular Dynamics Simulations. *J. Comput. Chem.* **1990**, *11*, 700–733.

(14) Loncharich, R. J.; Brooks, B. R.; Pastor, R. W. Langevin Dynamics of Peptides: The Frictional Dependence of Isomerization Rates ofN-Acetylalanyl-N?-Methylamide. *Biopolymers* **1992**, *32*, 523–535.

(15) Cui, Q.; Elstner, M.; Kaxiras, E.; Frauenheim, T.; Karplus, M. A QM/MM Implementation of the Self-Consistent Charge Density Functional Tight Binding (SCC-DFTB) Method. *J. Phys. Chem. B* **2000**, *105*, 569–585.

(16) Bowman, A. L.; Grant, I. M.; Mulholland, A. J. QM/MM Simulations Predict a Covalent Intermediate in the Hen Egg White Lysozyme Reaction with Its Natural Substrate. *Chem. Commun.* **2008**, *0*, 4425.

(17) Woods, C. J.; Malaisree, M.; Hannongbua, S.; Mulholland, A. J. A Water-Swap Reaction Coordinate for the Calculation of Absolute Protein–ligand Binding Free Energies. *J. Chem. Phys.* **2011**, *134*, 54114.